Characterization of Tau ELISAs for Evaluating Tau Accumulation in the Brains With Alzheimer's Disease

Mitsuru Shinohara (shinohara@ncgg.go.jp)
Department of Aging Neurobiology, Center for Development of Advanced Medicine for Dementia, National Center for Geriatrics and Gerontology, 7-430, Morioka, Obu, Aichi 474-8511, Japan https://orcid.org/0000-0003-3045-7338

Junko Hirokawa
National Center for Geriatrics and Gerontology

Akemi Shimodaira
National Center for Geriatrics and Gerontology

Yoshitaka Tashiro
National Center for Geriatrics and Gerontology

Kaoru Suzuki
National Center for Geriatrics and Gerontology

Akio Fukumori
National Center for Geriatrics and Gerontology

Tomoyasu Matsubara
Tokyo Metropolitan Geriatric Hospital and Institute of Gerontology: Tokyo-to Kenko Choju Iryo Center

Maho Morishima
Tokyo Metropolitan Geriatric Hospital and Institute of Gerontology: Tokyo-to Kenko Choju Iryo Center

Yuko Saito
Tokyo Metropolitan Geriatric Hospital and Institute of Gerontology: Tokyo-to Kenko Choju Iryo Center

Shigeo Murayama
Tokyo Metropolitan Geriatric Hospital and Institute of Gerontology: Tokyo-to Kenko Choju Iryo Center

Naoyuki Sato
National Center for Geriatrics and Gerontology

Research

Keywords: tau, ELISA, brain, Alzheimer's disease

Posted Date: January 20th, 2021

DOI: https://doi.org/10.21203/rs.3.rs-149164/v1

Abstract

Background: One main pathological hallmark of Alzheimer's disease (AD) is tau accumulation as neurofibrillary tangles (NFTs) in the brain. Although sandwich enzyme-linked immunosorbent assays (ELISAs) are useful for quantifying tau levels, including those in CSF, plasma and brain, it has not yet been determined which antibody combination is the most appropriate for assessing the neuropathological accumulation of tau in the brain.

Methods: We developed several sandwich tau ELISAs by introducing antibodies against several tau epitopes, including from its N-terminal and C-terminal regions, and evaluated tau levels depending on disease stage, brain areas, and other AD-related changes.

Results: We observed that tau levels in insoluble brain fraction determined by each ELISAs differ depending on the epitopes of the antibodies: there is a trend that non-AD control samples yield relatively high signals when an antibody against the N-terminal region of tau is used. On the other hand, ELISAs combining two antibodies against the later-middle to C-terminal regions of tau produced substantially increased signals from AD samples, compared to those from non-AD controls. Such ELISAs better distinguish AD and non-AD controls, and the results are more closely associated with Braak NFT stage, Aβ accumulation, and neuroinflammatory markers. In addition, these ELISAs can reflect the pattern of tau spread across brain regions.

Conclusions: Tau ELISAs that combine two antibodies against the later-middle to C-terminal regions of tau can better reflect neuropathological tau accumulation, which would enable to evaluate tau accumulation in the brain at a biochemical level.

Background

Alzheimer's disease (AD) is neuropathologically characterized by the accumulation of amyloid-β (Aβ) peptides and tau proteins, which appear as amyloid plaques and neurofibrillary tangles (NFTs), respectively. It is widely recognized that neuronal loss and clinical severity correlate more with NFTs than amyloid plaques, suggesting that NFTs play major roles in the onset of dementia (1). Together with many failures in clinical trials targeting Aβ, tau has attracted more attention as a key player and a therapeutic target for AD (2–6). Therefore, accurate measurement of tau accumulation has become more critical in the assessment of the disease progression and the efficacy of therapies that target tau.

To evaluate tau accumulation in the brain, several methods have been developed, including histochemical, immunohistochemical, biochemical, and radiological methods. While several modifications exist, silver impregnation techniques, such as Bielschowsky staining and the modified Gallyas method, are the standard methods by which neuropathologists observe NFTs and define Braak stages (7–9). However, non-silver impregnation staining methods, such as thioflavin-S staining, are also used by some neuropathologists for the neuropathological assessment of NFTs due to its simplicity, consistency, and cost-effectiveness (10–12). Immunohistochemical methods that use antibodies against phosphorylated or aggregated tau are very specific and sensitive in identifying NFTs; thus, these methods are also frequently used to obtain information that complements the results of histochemical staining despite some disadvantages, such as high cost and epitope loss in advanced NFTs (13–16). Biochemical methods, such as western blotting and mass spectrometry, have contributed to characterizing tau accumulation in details at the molecular level, but they are rarely used for diagnostic purpose (17–20). On the other hand, recently developed tau PET imaging techniques have significant advantages for detecting NFTs as to potentially determine the Braak stage in antemortem brains, although off-target binding effects should be considered (21–23).

The sandwich ELISA is a generally very quantitative biochemical method, enabling us to preciously evaluate even subtle changes in protein levels. For example, Aβ ELISAs are one of gold standard methods used to evaluate the degree of Aβ

accumulation in the brain as well as the subtle changes in biofluids (24–29). On the other hand, although tau ELISAs are used to measure change in tau levels in CSF or blood (29–32), they are rarely used to evaluate the amount of tau accumulation in the brain. To begin to use tau ELISAs to evaluate tau accumulation in the brain, it should be considered that the reactivity of these ELISAs could be very different depending on the epitopes recognized by antibodies, similar to the results obtained in evaluation of tau in CSF (32). Thus, by using several antibodies against N-terminal to C-terminal regions of tau, this study aims to identify the appropriate set of antibodies for use in tau ELISAs to evaluate neuropathological tau accumulation in the brain.

Methods

Human brain tissues— Postmortem brain tissues were obtained from the Brain Bank for Aging Research (BBAR) at the Tokyo Metropolitan Geriatric Hospital and Institute of Gerontology under the approval of the institutional ethics committees. The BBAR routinely performs the standardized neuropathological evaluations as previously described (33, 34). In the first cohort, we analyzed the gray matter of the frontal cortex (Brodmann area (BA) = 8 or 9) of 24 AD patients and 36 non-AD controls whose demographics are shown in Supplementary Table 1. In the second cohort, we analyzed five neocortical areas (dorsolateral prefrontal (BA = 9), orbitofrontal (BA = 12), inferior temporal (BA = 20), inferior parietal (BA = 39/40), and primary visual (BA = 17)), four limbic areas (posterior cingulate (BA = 31), entorhinal (BA = 28), amygdala, and insular), and five subcortical areas (striatum (caudate), thalamus, cerebellum, diagonal band of Broca, and nucleus accumbens) of 18 individuals; these individuals included 5 normal elderly controls, 4 cases with plaque dominant senile change (PSC), 4 cases with NFT-predominant change (NFTC), and 5 AD cases. AD was defined according to the BBAR definition (Braak NFT stage ≥ IV and Braak senile plaque stage = C (or 3)) and the presence of clinical dementia (35). Among the cases who did not meet the criteria of AD, cases who had severe senile plaques (Braak senile plaque stage ≥ B (or 2)) were diagnosed with PSC (plaque dominant senile change), and cases who had significant NFT pathology (Braak NFT stage ≥ III) without severe senile plaques (Braak SP stage ≤ A (0 or 1)) were diagnosed with NFTC (NFT-predominant change) (36).

Sample preparation— We extracted proteins according to a previously-described method with some modifications (37–40). In brief, after the removal of meninges and blood vessels, brain specimens were pulverized in a prechilled (on dry ice) BioPulverizer (BioSpec) and homogenized with a polytron homogenizer (Kinematica) at a ratio of 10 ml/g of wet-weight brain tissue in ice-cold RIPA lysis buffer (Millipore) containing 0.1% SDS, a complete protease inhibitor cocktail, and PhosSTOP phosphatase inhibitor cocktail (Roche) on ice. In a small pilot study, we also extracted brain tissue in ice-cold TBS with 1% Sarkosyl (Merck) containing a complete protease inhibitor cocktail, and PhosSTOP phosphatase inhibitor cocktail (Roche), instead of RIPA lysis buffer. After centrifugation at 100,000 g for 1 hour at 4 °C, the supernatant was aliquoted and stored at -80 °C (referred to as the RIPA-soluble fraction if RIPA was used, or the Sarkosyl-soluble fraction if Sarkosyl was used). The residual pellet was rehomogenized in TBS plus 5 M guanidine hydrochloride (GuHCl), pH 7.6, and incubated with mild agitation for 12–16 hour at room temperature. After centrifugation at 15,000 g for 30 minutes, the resultant supernatant (referred to as the GuHCl fraction, or RIPA-insoluble fraction if RIPA was used or the Sarkosyl-insoluble fraction if Sarkosyl was used) was diluted with 9 volumes of TBS, aliquoted and stored at -80 °C until the analysis by ELISA.

Tau ELISAs—Tau (or total-tau) ELISAs were developed by combining several commercially available antibodies as follows: Tau13 (epitope: 20–35 a.a. of Tau-441, Biolegend), HT7 (epitope: 159–163 a.a. of Tau-441, Thermo Scientific), Tau5 (epitope: 218–225 a.a. of Tau-441, Biolegend), 77G7 (epitope: 316–335 a.a. of Tau-441, Biolegend), OST (OST00329W, epitope: 323–363 a.a. of Tau-441, Osences), and Tau46 (epitope: 404–441 a.a. of Tau-441, Biolegend). One of these antibodies was used for capture, and the other antibody conjugated to biotin was used for detection. Recombinant human Tau-441 protein (Wako) was used as a standard. We also developed an ELISA against phosphorylated forms of tau (phospho-tau) by using Tau5 as a capture antibody and the biotin-conjugated mouse

monoclonal AT270 antibody (epitope: phospho-tau 181, Thermo Scientific) as a detection antibody. Synthetic peptides were generated: “TPPAPKT(p)PPSSGEPPPSLPTPPTREPKKVA” consisted of two partial fragments from 175 a.a. to 189 a.a. of Tau-441 including phosphorylated- threonine at 181 a.a. (corresponding to the residue of Tau-441), and from 213 a.a. to 227 a.a. of Tau-441. This peptide was used as standards. Colorimetric quantification was performed using an iMark plate reader (Bio-Rad) after incubations with horseradish peroxidase (HRP)-linked Avidin-D (Vector) or streptavidin-PolyHRP40 (Stereospecific Detection Technologies), followed by incubation with 3,3’,5,5’-tetramethylbenzidine substrate (Nacalai Tesque, Kyoto, Japan).

Quantification of other proteins—The levels of full-length Aβ40 ($Aβ_{1-40}$) and Aβ42 ($Aβ_{1-42}$), glial fibrillary acidic protein (GFAP), CD11b, and apoE were determined by ELISA as previously described (37, 38, 40). The RIPA-insoluble (GuHCl) fraction was used to measure Aβ40, Aβ42, and apoE levels, and the RIPA-soluble fraction was used to measure the GFAP, and CD11b levels. The levels of the total proteins in each fraction were determined by a Protein Assay BCA kit according to the manufacturer’s instructions (Fujifilm).

Western blotting—GuHCl fraction samples were first dialyzed with 8 M urea before electrophoresis. The samples were mixed with 4x Laemmli Sample Buffer (BIO-RAD) and were run on the Tris-Glycine electrophoresis system (NIHON EIDO Co., Ltd.). The immunoreactive bands by each tau antibody and the appropriate HRP-conjugated secondary antibodies were detected and quantified using a chemiluminescent imaging system, ImageQuant LAS 3000 (Fujifilm).

Statistical analysis —All the values measured by ELISAs were first normalized to the total protein levels in the sample. Comparisons of these normalized values between AD cases and non-AD controls were performed by the Wilcoxon signed-rank test. The nonparametric Spearman rank correlation coefficient was used to summarize the degree of correlation between tau levels and neuropathological or biochemical measurements. ROC (receiver operating characteristic) curve analyses were performed considering AD as an event. All the statistical analyses were performed by JMP Pro (version 13.0.0; SAS, Cary, NC). *P*-values of less than 0.05 were considered significant.

Results

Pilot tests of tau ELISAs to analyze the brains of AD patients and non-AD controls.

We developed several tau ELISAs by combining several antibodies against epitopes raging from the N-terminal to C-terminal regions of tau (Fig. 1A). All these ELISAs showed good dose-dependent standard curves using recombinant human tau-441 protein (Supplementary Fig. 1). We then tested samples pooled from the RIPA-insoluble fraction (i.e., GuHCl fraction) of the frontal cortex of 8 individuals with AD or without AD (control) by using these ELISAs. The results are summarized in Fig. 1B. When antibodies against the N-terminal to middle regions of tau were used in ELISA, the control sample showed relatively high levels of tau. In particular, including an antibody against the N-terminal region (i.e., Tau13) showed relatively high tau levels (25–400 ng/mg). In the ELISAs using Tau13 antibody, a mild difference between the control and AD samples was observed; AD sample showed approximately 1.2- to 5-fold higher levels of tau than those in the control sample. On the other hand, when antibodies against the middle to C-terminal regions of tau were used, the control sample showed relatively low levels of tau (below 100 ng/mg). More importantly, when antibodies against the later-middle (i.e., 218–225 a.a. of Tau-441: epitope of Tau5 antibody) to C-terminal regions of tau were combined, substantial differences between the control and AD samples were generally observed; AD sample showed more than 10- to 100-fold higher levels of tau than the control sample. These results suggest that tau ELISAs have different reactivities depending on the epitopes targeted by tau antibodies, which might affect the evaluation of tau pathology in brains of AD patients.

Detailed comparison of tau ELISAs to distinguish the brains of AD patients and non-AD controls.

To confirm our pilot results, we next analyzed individual RIPA-insoluble fraction of frontal cortex of AD and non-AD control brains (n = 60, Supplementary Table. 1) by using representative tau ELISAs that used Tau13 (epitope: N-terminal 20–35 a.a. of Tau-441) or OST (epitope: MTBR 323–363 a.a. of Tau-441) as the capture antibody. The results are shown in Fig. 2A. When Tau13 was used as a capture antibody, the brains of control cases showed relatively higher levels of tau (100–600 ng/mg, also shown in Supplementary Table 2), and the brains of AD patients showed 1.5- to 4-fold increases in tau levels, compared to those in control brains; moreover, this difference was not always significant. When OST was ued as a capture antibody, the brains of control cases showed relatively lower levels of tau, especially when antibodies against the middle to C-terminal regions of tau were used as detection antibodies (less than 100 ng/mg, also shown in Supplementary Table 2). Moreover, consistent with our initial results, ELISAs using antibodies against the later-middle to C-terminal regions showed robust differences between control and AD; the brains of AD patients had over 500-fold higher levels of tau accumulation than the brains of controls (also shown in Supplementary Table 2). To confirm that ELISAs using antibodies against the later-middle to C-terminal regions of tau would be better to distinguish AD patients and non-AD controls, we performed ROC curve analyses. Indeed, when OST antibody was used as a capture antibody and antibodies against the middle to C-terminal regions of tau were used as detection antibodies, the AUC was more than 0.96 (Fig. 2B). In particular, OST-77G7 ELISA showed the best result (AUC = 0.97). On the other hand, when Tau 13 was used as a capture antibody, the AUC was relatively lower, ranging from 0.65 to 0.79, and Tau13-Tau5 ELISA yielded the lowest AUC value (AUC = 0.65). The significant difference in AUC between each ELISA is described in detail in Supplementary Table 3. These results confirm that tau ELISAs using antibodies against the later-middle to C-terminal regions of tau can better distinguish AD patients and non-AD controls.

We also analyzed the RIPA-soluble fraction to determine how far this easily-extractable fraction can distinguish AD and non-AD controls by these ELISAs. We tested OST-77G7 and Tau13-Tau5 ELISAs, which showed the best and worst AUC, respectively, for the RIPA-insoluble fraction. When tested by Tau13-Tau5 ELISA, the control cases and AD patients showed almost similar values without a significant difference ($p = 0.1283$, Supplementary Fig. 2A). On the other hand, when tested by OST-77G7 ELISA, AD patients showed a significant approximately 1.5-fold increase (median value) in tau levels ($p = 0.0053$, Supplementary Fig. 2A). Notably, in OST-77G7 ELISA, a strong correlation was observed ($r = 0.85$) between RIPA-soluble tau and RIPA-insoluble tau, while the RIPA-soluble tau levels in some AD patients overlapped with those of controls (Supplementary Fig. 2B). Indeed, in the ROC curve analysis to distinguish AD patients and non-AD controls, the AUC was 0.72 (Supplementary Fig. 2C), which was weaker than that of the GuHCl fraction. These results indicate that the RIPA-insoluble (i.e., GuHCl) fraction is more suitable than the RIPA-soluble fraction for distinguishing AD patients and non-AD controls by this tau ELISA.

To assess whether other popular extraction methods, such as using Sarkosyl instead of RIPA, give a similar result, we also tested the Sarkosyl-insoluble fraction from a small number of subjects. In OST-77G7 ELISA, AD samples showed significantly higher Sarkosyl-insoluble tau levels than non-AD control samples ($p = 0.0003$), while in Tau13-Tau5 ELISA, there was no significant difference between these samples ($p = 0.1046$) (Supplementary Fig. 3A). Notably, tau levels in the Sarkosyl-insoluble fraction measured by OST-77G7 ELISA correlated well with tau levels in the RIPA-insoluble fraction measured by the same OST-77G7 ELISA (Supplementary Fig. 3C); in addition, these results showed good AUC values (AUC = 0.97) for distinguishing AD patients and non-AD controls, similar to those of the RIPA-insoluble fraction (Supplementary Fig. 3D). These results indicate that our findings can be applied to other popular extraction methods, including a method using Sarkosyl.

Correlation of tau ELISA results with NFT neuropathological stage and other AD-related neurodegenerative markers.

To determine whether these tau ELISAs indeed reflect tau accumulation in the brain, we analyzed the correlation between Braak NFT stage and tau levels in the RIPA-insoluble fraction determined by each ELISA. The results are summarized in Table 1. When Tau13 was used as the capture antibody, we observed mild-to-moderate correlations between tau levels

by ELISA and Braak NFT stage (r = 0.35–0.67). In particular, tau levels measured by Tau13-Tau5 ELISA showed the lowest correlation (r = 0.35, p = 0.056, Fig. 3A). On the other hand, with ELISAs using OST as a capture antibody, we obtained better correlations with Braak NFT stage, especially when detection antibodies against the later-middle to C-terminal regions of tau were used (r > 0.80), including OST-77G7 ELISA (r = 0.81, p < 0.001, Fig. 3D). These findings indicate that tau ELISAs using antibodies against the later-middle region to C-terminal regions of tau can better reflect the pathological accumulation of tau in the brain.

Table 1
Correlation between tau levels determined by each ELISAs and Aβ, synaptic/ neuronal markers, and other neurodegenerative markers.

	AUC	Braak NFT		Aβ1–40		Aβ1–42		GFAP		CD11b		ApoE GuHCl	
Tau ELISA		r	p-value	r	p-value	r	p-value	r	p-value	r	p-value	r	p-value
Tau13-HT7	0.79	0.55	< 0.001	0.39	0.017	0.23	0.753	0.16	1.00	0.12	1.00	0.34	0.058
Tau13-Tau5	0.65	0.35	0.056	0.21	0.942	0.26	0.438	0.09	1.00	0.01	1.00	0.21	0.941
Tau13-77G7	0.76	0.53	< 0.001	0.42	0.008	0.46	0.004	0.19	1.00	0.10	1.00	0.37	0.029
Tau13-Tau46	0.76	0.50	< 0.001	0.43	0.005	0.52	< 0.001	0.04	1.00	-0.01	1.00	0.37	0.031
OST-Tau13	0.84	0.67	< 0.001	0.50	< 0.001	0.41	0.014	0.21	0.924	0.26	0.408	0.43	0.005
OST-HT7	0.9	0.73	< 0.001	0.67	< 0.001	0.70	< 0.001	0.23	0.699	0.09	1.00	0.53	< 0.001
OST-Tau5	0.96	0.82	< 0.001	0.63	< 0.001	0.50	< 0.001	0.38	0.023	0.30	0.181	0.53	< 0.001
OST-77G7	0.97	0.81	< 0.001	0.65	< 0.001	0.49	< 0.001	0.45	0.003	0.42	0.008	0.60	< 0.001
OST-Tau46	0.96	0.83	< 0.001	0.64	< 0.001	0.64	< 0.001	0.26	0.379	0.20	1.00	0.55	< 0.001

We also analyzed the correlation with the levels of Aβ, inflammatory cell markers, GFAP and CD11b, and apoE protein. These results are also summarized in Table 1, and representative results of the correlations of Tau13-Tau5 ELISA, and OST-77G7 ELISA are also shown as graphs in Fig. 3B, C, E, and F. In brief, while both Aβ40 and Aβ42 in the GuHCl fraction were increased in the brains of AD patients (Supplementary Table 2), Aβ40 in particular tended to have a better correlation with tau levels measured by ELISAs that combined antibodies against the middle region to C-terminal regions of tau (r > 0.60), likely because Aβ40 increases during AD progression while Aβ42 reaches a plateau at an early stage (39). Regarding inflammatory markers, we confirmed that the levels of inflammatory cell markers tended to be increased in AD patients compared to controls (GFAP levels were significant, but CD11b levels only exhibited a trend, Supplementary Table 2). The results of the ELISAs using Tau13 as a capture antibody were generally not well correlated with the levels of glial markers (GFAP: r = 0.04–0.19; CD11b: r = -0.01–0.12). On the other hand, the results of ELISAs using OST as a capture antibody tended to be better correlated with the levels of these markers (GFAP: r = 0.21–0.45; CD11b: r = 0.09–0.42). In particular, their correlations with tau levels measured by OST-77G7 ELISA were significant (GFAP: r = 0.45, p = 0.003; CD11b: r = 0.42, p = 0.008). It is known that apoE accumulates on NFTs, especially extracellular NFTs (41, 42), in addition to amyloid plaques. Since accumulated apoE could be evaluated in the GuHCl fraction (38), we

analyzed the correlation with apoE levels in the GuHCl fraction, and we observed that the apoE levels were better correlated with tau levels measured by ELISAs using OST as a capture antibody (r = 0.43–0.60), rather than those using Tau13 (r = 0.21–0.37). These results indicate that Tau ELISAs with antibodies against the later-middle to C-terminal regions of tau (especially OST-77G7 ELISA) can better reflect AD-associated pathological changes, including Aβ, inflammatory cells, and apoE accumulation in addition to tau accumulation.

Distinct reactivity of tau antibodies by western blotting analysis

To address the reason why ELISA results are different depending on the epitopes targeted by tau antibodies, we performed western blotting analysis. In the GuHCl fraction, tau was generally detected as the monomer form (50–64 kDa) and aggregated form (> 64 kDa) by western blotting (Fig. 4A). When an antibody against the N-terminal region of tau was used (i.e., Tau13), there was a trend that the monomer form of tau was more clearly visible than its aggregated form. On the other hand, when antibodies against the middle to C-terminal regions of tau were used, the aggregated form was clearly observed in AD patients, especially with antibodies against MTBR to the C-terminal region of tau (i.e., 77G7 and Tau46); these results were confirmed by densitometric analysis (Fig. 4B). These difference in the reactivity of tau depending on antibody recognition of epitopes from the N-terminal to C-terminal regions of tau might explain the observed difference in the ELISA results.

Tau accumulation across brain regions during disease development

To address whether these tau ELISAs can evaluate the pattern of tau spread during AD development, we analyzed multiple brain regions of 18 individuals with different stages of AD (demographic information of each case is shown in Supplementary Table 4). We used OST-77G7 ELISA as one of the best tau ELISAs. Results are shown in each individual case (Fig. 5). Indeed, AD patients showed increased insoluble tau levels in several brain regions, including the limbic areas and neocortical areas, but less remarkable levels in several subcortical areas, including the striatum and thalamus, and cerebellum. On the other hand, individuals with early AD pathology (PSC or NFTC), showed increased insoluble tau levels only in the entorhinal cortex, but not apparent in other brain regions. Interestingly, some of these individuals showed somewhat increased insoluble tau levels in the amygdala and temporal cortex, although the extent of tau levels was much fewer compared to that in the entorhinal cortex. The control groups (Braak NFT stage I) generally showed low insoluble tau levels. Notably, one individual showed apparent insoluble tau levels in the entorhinal cortex (Cont#5). When Tau13-Tau5 ELISA was used, there were no such trends recapitulating the progression of Braak NFT stage (Supplementary Fig. 4). These results indicate that OST-77G7 ELISA can address the pattern of tau spread pattern across brain regions during AD development.

Discussion

Compared to biomarker studies that analyze tau levels in CSF or plasma, the number of studies utilizing ELISAs to detect tau accumulation in brains is much smaller. However, previous studies exist that used ELISAs to detect tau levels in the brain (43–49). Direct ELISAs, where brain homogenate or purified paired helical filament (PHF) is coated on microwells and then detected by anti-tau antibodies, were first developed by several groups (43–46). One major disadvantage of direct ELISAs is high background signals due to the nonspecific binding of samples to the plate, which could overestimate or underestimate the amount of target proteins even if standard proteins are used. Indeed, most of these studies neither used standard proteins nor calculated tau levels (44–46). Sandwich ELISAs have also been developed by some researchers to detect phosphorylated tau levels in the brain (47–49). However, they used a buffer -soluble (i.e., no detergent) fraction of brain tissue, which might significantly underestimate the amount of tau accumulation that is highly insoluble (50). Additionally, some phospho-specific tau antibodies could lose their epitope in the advanced stage of NFT formation (14, 16, 51, 52). On the other hand, there are few studies using sandwich ELISAs to detect

accumulation of total tau (i.e., using buffer- or detergent-insoluble fractions) in the brain, except for our previous study that used OST-HT7 ELISA (38). However, our previous study also did not elucidate whether OST-HT7 ELISA is the best option, or whether other ELISAs exist that can better evaluate neuropathological tau accumulation.

Thus, the current study comprehensively compared combinations of tau antibodies, and observed that ELISAs using antibodies, especially against MTBR to C-terminal regions of tau can assess neuropathological tau accumulation that well distinguish AD patients and non-AD controls, and correlate with Braak NFT stage, Aβ accumulation, and neuroinflammation. Our results appear to be consistent with the previous studies showing that MTBR to C-terminal regions form a core and aggregate as PHF, while the N-terminal region is easily truncated (20, 53). Interestingly, secreted tau in the CSF or cellular medium mostly loses its C-terminal regions, likely from the region corresponding to the epitope of Tau5 (54, 55). This truncation physiologically occurs irrespective of the disease, while Aβ accumulation would promote the secretion (55, 56). Although previous studies have observed that tau ELISAs using a C-terminal antibody are not appropriate for detecting secreted tau in CSF (32), it would be interesting to examine whether the currently optimal ELISAs to detect tau in the brain, such as OST-77G7 ELISA, indeed cannot detect tau levels in CSF.

Western blotting analyses showed a clear difference in the reactivity of each tau antibody with aggregated tau and monomer tau in the insoluble fraction of brains: the reactivity of aggregated tau to monomer tau is increased from antibodies targeting the N-terminal epitope to antibodies targeting the C-terminal epitope (Fig. 4), which likely explains the difference in reactivity of each ELISA. One plausible explanation for this result is that antibodies targeting the N-terminal epitope of tau cannot recognize aggregated tau due to the absence of the N-terminal region (20, 53). Additionally, monomer tau in the insoluble fraction appears to be less recognized by antibodies against the middle to C-terminal regions of tau, compared to an antibody against the N-terminal region, suggesting that the middle to C-terminal regions of monomer tau in the insoluble fraction would be masked for unknown reasons. Further studies are necessary to address the mechanism.

One advantage of sandwich ELISAs is their quantitative feature. The Braak NFT staging system assigns seven stages based on the topological distribution of tau, with the limitation that such a semiquantitative method is insufficient to precisely estimate the degree of tau accumulation in each area (16). Indeed, we observed a wide range of tau levels with OST-77G7 ELISA among AD patients with the same Braak stage VI (in the frontal cortex of the first cohort: 1,630 to 245,100 ng/mg, Supplementary Table 2). Notably, a few control individuals pathologically diagnosed by Braak NFT stage I indeed had a significant amount of tau accumulation in the entorhinal cortex (Fig. 5), suggesting that our ELISA method could be more sensitive for detecting neuropathological tau accumulation in the brain than conventional pathological assessment. In future studies, it would be interesting to address its relationship with cognitive decline, disease progression, and other tauopathies. Nonetheless, this method would be useful to determine the degree of pathological tau accumulation, in addition to the diagnosis of neuropathological Braak stage.

By analyzing multiple brain regions, we observed that the pattern of tau spread is consistent with the scheme of Braak NFT stage: tau first accumulate in the entorhinal cortex (Braak stage I-II), then involves the limbic area or its-surrounding areas (Braak stage III-VI), and finally reaches neocortical areas (Braak stage V-VI) (8). Such analysis of region-specific patterns of AD pathologies would provide important insights into the pathological mechanism of the disease, as shown in our recent studies focusing on Aβ accumulation (37–39, 57). Thus, when combined with additional data, such as region-specific Aβ data or comprehensive gene expression data, the current data would be useful to address the pathological mechanism of region-specific tau accumulation as well as the crosstalk between Aβ and tau accumulation.

Limitations

One potential limitation in the current study is the lack of evaluation of phospho-tau accumulation. In general, it is difficult to evaluate phosphorylated proteins in postmortem brains due to their instability through dephosphorylation during autopsy, sample storage or extraction processes (58–60). Notably, some phospho-tau epitopes might also be lost in the advanced stage of NFT formation (14, 16, 51, 52). Despite such disadvantages, we tested one phospho-tau ELISA using AT270 antibody, which is widely used to detect phospho-tau in CSF and plasma (32, 61, 62). This phospho-tau ELISA indeed showed weaker performance (AUC = 0.80) in distinguishing AD patients and non-AD controls, compared to total tau levels by OST-77G7 ELISA (Supplementary Fig. 5). Future studies are necessary to address whether other phospho-tau ELISAs also show different performances depending on the epitope targeted by the antibodies and to determine which total tau ELISA or phospho-tau ELISA is better for evaluating neuropathological tau accumulation.

Conclusions And Future Directions

In conclusion, we evaluated several total tau ELISA, and observed that ELISA combining antibodies against the later-middle to C-terminal regions of tau can better address neuropathological tau accumulation that associates with other neurodegenerative changes during AD development. The current finding proposes useful total tau ELISA methods for evaluating neuropathological tau accumulation in the brain, which will facilitate understanding the pathological mechanism as well as evaluating therapeutic efficacy in future studies focusing on tau accumulation.

Abbreviations

Aβ, β−amyloid; AD, Alzheimer’s disease; CERAD, Consortium to Establish a Registry for Alzheimer's Disease; ELISA, enzyme-linked immunosorbent assay; GFAP, glial fibrillary acidic protein; GuHCl, guanidine hydrochloride; MTBR, microtubule binding region; NFT, neurofibrillary tangles; PHF, paired helical filament; RIPA, radioimmunoprecipitation

Declarations

Ethical Approval and Consent to participate

This study was approved by the Tokyo Metropolitan Geriatric Hospital and Institute of Gerontology ethics committee and National Center for Geriatrics and Gerontology ethics committee. In compliance with the Declaration of Helsinki, written informed consent was obtained from all participants and their study partners/caregivers prior to study participation.

Consent for publication

All participants or study partners/caregivers gave written informed consent to participate in this study for scientific purposes, including publications. The informed consents are available from the corresponding author upon reasonable request. All reported data are anonymized, and no individual participant information can be identified from the presented datasets.

Availability of data and materials

All data generated or analysed during this study are included in this published article and its supplementary information files.

Competing interests

The authors declare that they have no competing interests.

Funding

This work was supported in part by the Research Funding for Longevity Sciences from the National Center for Geriatrics and Gerontology (19-18 to MS; 19-3 & 19-9 to NS; 20-6 to SM); Grants-in-Aid from Japan Promotion of Science (17H07419 & 18H02725 to MS; MEXT15K15272 & MEXT17H04154 to NS; JP 16H06277 (CoBiA) to SM & YS); AMED (JP20dm0107106 to SM); a Takeda Science Foundation Research Encouragement Grant (to MS); a research grant from the Japan Foundation For Aging And Health (to MS); a research grant from the Uehara Memorial Foundation (to MS); a research grant from the Hori Sciences and Arts Foundation (to MS) and a research grant from Yokoyama Foundation for Clinical Pharmacology (to MS).

Authors' contributions

M.S., and N.S. contributed to the concept and study design. M.S., J. H., A.S., Y.T., K.S., A.F., T.M., M.M., Y.S., S.M., and N.S. contributed to data acquisition and analysis. M.S. and N.S. contributed to drafting the manuscript and figures. All the authors edited and reviewed the final manuscript.

Acknowledgments

We would like to thank the laboratory members in the Department of Aging Neurobiology and Drs. Masato Hasegawa, Naruhiko Sahara, and Katsuhiko Yanagisawa for discussions.

Authors' information

Correspondence to Mitsuru Shinohara and Naoyuki Sato.

Affiliations

Department of Aging Neurobiology, Center for Development of Advanced Medicine for Dementia, National Center for Geriatrics and Gerontology, 7-430, Morioka, Obu, Aichi 474-8511, Japan

Mitsuru Shinohara, Junko Hirokawa, Akemi Shimodaira, Yoshitaka Tashiro, Kaoru Suzuki, Akio Fukumori & Naoyuki Sato

Department of Aging Neurobiology, Graduate School of Medicine, Osaka University, 2-2, Yamadaoka, Suita, Osaka 565-0871, Japan

Mitsuru Shinohara, Akio Fukumori & Naoyuki Sato

Department of Pharmacotherapeutics II, Osaka University of Pharmaceutical Sciences

4-20-1 Nasahara, Takatsuki, Osaka 569-1094, JAPAN

Akio Fukumori

Department of Neuropathology (the Brain Bank for Aging Research), Tokyo Metropolitan Geriatric Hospital and Institute of Gerontology, 35-2, Sakae-machi, Itabashi, Tokyo 173-0015, Japan

Tomoyasu Matsubara, Maho Morishima, Yuko Saito & Shigeo Murayama

Brain Bank for Neurodevelopmental, Neurological and Psychiatric Disorders, United Graduate School of Child Development, Osaka University, 2-2, Yamadaoka, Suita, Osaka, 565-0871, Japan

Shigeo Murayama

References

1. P. V. Arriagada, J. H. Growdon, E. T. Hedley-Whyte, B. T. Hyman, Neurofibrillary tangles but not senile plaques parallel duration and severity of Alzheimer's disease. *Neurology* **42**, 631-639 (1992).
2. K. R. Brunden, J. Q. Trojanowski, V. M. Lee, Advances in tau-focused drug discovery for Alzheimer's disease and related tauopathies. *Nature reviews. Drug discovery* **8**, 783-793 (2009).
3. E. E. Congdon, E. M. Sigurdsson, Tau-targeting therapies for Alzheimer disease. *Nature Reviews Neurology* **14**, 399-415 (2018).
4. K. Iqbal, F. Liu, C.-X. Gong, Recent developments with tau-based drug discovery. *Expert Opinion on Drug Discovery* **13**, 399-410 (2018).
5. M. A. Busche, B. T. Hyman, Synergy between amyloid-β and tau in Alzheimer's disease. *Nature Neuroscience*, (2020).
6. R. van der Kant, L. S. B. Goldstein, R. Ossenkoppele, Amyloid-β-independent regulators of tau pathology in Alzheimer disease. *Nature Reviews Neuroscience* **21**, 21-35 (2020).
7. A. Alzheimer, Über einen eigenartigen schweren Erkrankungsprozeß der Hirnrinde. *Neurolog Centralbl* **23**, 1129-1136 (1906).
8. H. Braak, E. Braak, Neuropathological stageing of Alzheimer-related changes. *Acta neuropathologica* **82**, 239-259 (1991).
9. N. Kuninaka *et al.*, Simplification of the modified Gallyas method. *Neuropathology* **35**, 10-15 (2015).
10. R. D. Terry *et al.*, Senile Dementia of the Alzheimer Type Without Neocortical Neurofibrillary Tangles. *Journal of Neuropathology & Experimental Neurology* **46**, 262-268 (1987).
11. A. Sun, X. V. Nguyen, G. Bing, Comparative Analysis of an Improved Thioflavin-S Stain, Gallyas Silver Stain, and Immunohistochemistry for Neurofibrillary Tangle Demonstration on the Same Sections. *Journal of Histochemistry & Cytochemistry* **50**, 463-472 (2002).
12. M. E. Murray *et al.*, Neuropathologically defined subtypes of Alzheimer's disease with distinct clinical characteristics: a retrospective study. *The Lancet Neurology* **10**, 785-796 (2011).
13. B. L. Wolozin, A. Pruchnicki, D. W. Dickson, P. Davies, A neuronal antigen in the brains of Alzheimer patients. *Science* **232**, 648 (1986).
14. E. Braak, H. Braak, E. M. Mandelkow, A sequence of cytoskeleton changes related to the formation of neurofibrillary tangles and neuropil threads. *Acta neuropathologica* **87**, 554-567 (1994).
15. C. A. Lasagna-Reeves *et al.*, Identification of oligomers at early stages of tau aggregation in Alzheimer's disease. *FASEB journal : official publication of the Federation of American Societies for Experimental Biology* **26**, 1946-1959 (2012).
16. H. Braak, I. Alafuzoff, T. Arzberger, H. Kretzschmar, K. Del Tredici, Staging of Alzheimer disease-associated neurofibrillary pathology using paraffin sections and immunocytochemistry. *Acta neuropathologica* **112**, 389-404 (2006).
17. N. Nukina, Y. Ihara, One of the Antigenic Determinants of Paired Helical Filaments Is Related to Tau Protein. *The Journal of Biochemistry* **99**, 1541-1544 (1986).
18. K. S. Kosik, C. L. Joachim, D. J. Selkoe, Microtubule-associated protein tau (tau) is a major antigenic component of paired helical filaments in Alzheimer disease. *Proceedings of the National Academy of Sciences* **83**, 4044 (1986).
19. M. Morishima-Kawashima *et al.*, Ubiquitin is conjugated with amino-terminally processed tau in paired helical filaments. *Neuron* **10**, 1151-1160 (1993).
20. S. Taniguchi-Watanabe *et al.*, Biochemical classification of tauopathies by immunoblot, protein sequence and mass spectrometric analyses of sarkosyl-insoluble and trypsin-resistant tau. *Acta neuropathologica* **131**, 267-280 (2016).

21. D. T. Chien *et al.*, Early Clinical PET Imaging Results with the Novel PHF-Tau Radioligand [F-18]-T807. *Journal of Alzheimer's Disease* **34**, 457-468 (2013).
22. M. Maruyama *et al.*, Imaging of Tau Pathology in a Tauopathy Mouse Model and in Alzheimer Patients Compared to Normal Controls. *Neuron* **79**, 1094-1108 (2013).
23. A. Leuzy *et al.*, Tau PET imaging in neurodegenerative tauopathies—still a challenge. *Molecular Psychiatry* **24**, 1112-1134 (2019).
24. N. Suzuki *et al.*, High tissue content of soluble beta 1-40 is linked to cerebral amyloid angiopathy. *The American journal of pathology* **145**, 452-460 (1994).
25. R. Motter *et al.*, Reduction of β-amyloid peptide42 in the cerebrospinal fluid of patients with Alzheimer's disease. *Annals of Neurology* **38**, 643-648 (1995).
26. A. Tamaoka *et al.*, Amyloid β protein 1–42/43 (Aβ 1–42/43) in cerebellar diffuse plaques: enzyme-linked immunosorbent assay and immunocytochemical study. *Brain Research* **679**, 151-156 (1995).
27. A. Tamaoka *et al.*, Amyloid β protein 42(43) in cerebrospinal fluid of patients with Alzheimer's disease. *Journal of the Neurological Sciences* **148**, 41-45 (1997).
28. S. D. Schmidt, M. J. Mazzella, R. A. Nixon, P. M. Mathews, Aβ measurement by enzyme-linked immunosorbent assay. *Methods in molecular biology (Clifton, N.J.)* **849**, 507-527 (2012).
29. K. Blennow, A Review of Fluid Biomarkers for Alzheimer's Disease: Moving from CSF to Blood. *Neurol Ther* **6**, 15-24 (2017).
30. M. Vandermeeren *et al.*, Detection of tau proteins in normal and Alzheimer's disease cerebrospinal fluid with a sensitive sandwich enzyme-linked immunosorbent assay. *Journal of neurochemistry* **61**, 1828-1834 (1993).
31. H. Zetterberg *et al.*, Plasma tau levels in Alzheimer's disease. *Alzheimer's Research & Therapy* **5**, 9 (2013).
32. J. E. Meredith Jr *et al.*, Characterization of Novel CSF Tau and ptau Biomarkers for Alzheimer's Disease. *PLOS ONE* **8**, e76523 (2013).
33. M. Ikemura *et al.*, Lewy Body Pathology Involves Cutaneous Nerves. *Journal of Neuropathology & Experimental Neurology* **67**, 945-953 (2008).
34. Y. Saito, S. Murayama, Neuropathology of mild cognitive impairment. *Neuropathology* **27**, 578-584 (2007).
35. S. Murayama, Y. Saito, Neuropathological diagnostic criteria for Alzheimer's disease. *Neuropathology* **24**, 254-260 (2004).
36. A. Uchino *et al.*, Incidence and extent of TDP-43 accumulation in aging human brain. *Acta neuropathologica communications* **3**, 35 (2015).
37. M. Shinohara, R. C. Petersen, D. W. Dickson, G. Bu, Brain regional correlation of amyloid-beta with synapses and apolipoprotein E in non-demented individuals: potential mechanisms underlying regional vulnerability to amyloid-beta accumulation. *Acta neuropathologica* **125**, 535-547 (2013).
38. M. Shinohara *et al.*, Regional distribution of synaptic markers and APP correlate with distinct clinicopathological features in sporadic and familial Alzheimer's disease. *Brain* **137**, 1533-1549 (2014).
39. M. Shinohara *et al.*, Distinct spatiotemporal accumulation of N-truncated and full-length amyloid-β42 in Alzheimer's disease. *Brain* **140**, 3301-3316 (2017).
40. M. Shinohara *et al.*, Increased levels of Aβ42 decrease the lifespan of ob/ob mice with dysregulation of microglia and astrocytes. *FASEB journal : official publication of the Federation of American Societies for Experimental Biology* **34**, 2425-2435 (2020).
41. Y. Namba, M. Tomonaga, H. Kawasaki, E. Otomo, K. Ikeda, Apolipoprotein E immunoreactivity in cerebral amyloid deposits and neurofibrillary tangles in Alzheimer's disease and kuru plaque amyloid in Creutzfeldt-Jakob disease.

*Brain Res***541**, 163-166 (1991).

42. H. Yamaguchi *et al.*, Presence of apolipoprotein E on extracellular neurofibrillary tangles and on meningeal blood vessels precedes the Alzheimer beta-amyloid deposition. *Acta neuropathologica***88**, 413-419 (1994).
43. R. Rubenstein *et al.*, Paired helical filaments associated with Alzheimer disease are readily soluble structures. *Brain Res***372**, 80-88 (1986).
44. C. B. Caputo *et al.*, Immunological characterization of the region of tau protein that is bound to Alzheimer paired helical filaments. *Neurobiology of aging***13**, 267-274 (1992).
45. D. W. Dickson *et al.*, Correlations of synaptic and pathological markers with cognition of the elderly. *Neurobiology of aging***16**, 285-298 (1995).
46. V. Haroutunian, P. Davies, C. Vianna, J. D. Buxbaum, D. P. Purohit, Tau protein abnormalities associated with the progression of alzheimer disease type dementia. *Neurobiology of aging***28**, 1-7 (2007).
47. H. A. Ghanbari, T. Kozuk, B. E. Miller, S. Riesing, A sandwich enzyme immunoassay for detecting and measuring Alzheimer's disease–associated proteins in human brain tissue. *Journal of clinical laboratory analysis***4**, 189-192 (1990).
48. O. Condamines *et al.*, New immunoassay for the mapping of neurofibrillary degeneration in Alzheimer's disease using two monoclonal antibodies against human paired helical filament tau proteins. *Neuroscience Letters***192**, 81-84 (1995).
49. M. Herrmann *et al.*, ELISA-quantitation of phosphorylated tau protein in the Alzheimer's disease brain. *European neurology***42**, 205-210 (1999).
50. D. J. Selkoe, Y. Ihara, F. J. Salazar, Alzheimer's disease: insolubility of partially purified paired helical filaments in sodium dodecyl sulfate and urea. *Science***215**, 1243-1245 (1982).
51. M. Bobinski *et al.*, Duration of neurofibrillary changes in the hippocampal pyramidal neurons. *Brain Res***799**, 156-158 (1998).
52. P. Cras *et al.*, Extracellular neurofibrillary tangles reflect neuronal loss and provide further evidence of extensive protein cross-linking in Alzheimer disease. *Acta Neuropathol***89**, 291-295 (1995).
53. A. L. Guillozet-Bongaarts *et al.*, Tau truncation during neurofibrillary tangle evolution in Alzheimer's disease. *Neurobiology of aging***26**, 1015-1022 (2005).
54. N. R. Barthélemy *et al.*, Differential Mass Spectrometry Profiles of Tau Protein in the Cerebrospinal Fluid of Patients with Alzheimer's Disease, Progressive Supranuclear Palsy, and Dementia with Lewy Bodies. *Journal of Alzheimer's disease : JAD***51**, 1033-1043 (2016).
55. C. Sato *et al.*, Tau Kinetics in Neurons and the Human Central Nervous System. *Neuron***97**, 1284-1298.e1287 (2018).
56. N. Mattsson-Carlgren *et al.*, Aβ deposition is associated with increases in soluble and phosphorylated tau that precede a positive Tau PET in Alzheimer's disease. *Science Advances***6**, eaaz2387 (2020).
57. Y. Yamazaki *et al.*, Selective loss of cortical endothelial tight junction proteins during Alzheimer's disease progression. *Brain***142**, 1077-1092 (2019).
58. Y. Wang *et al.*, Rapid alteration of protein phosphorylation during postmortem: implication in the study of protein phosphorylation. *Sci Rep***5**, 15709-15709 (2015).
59. J. Li, T. D. Gould, P. Yuan, H. K. Manji, G. Chen, Post-mortem Interval Effects on the Phosphorylation of Signaling Proteins. *Neuropsychopharmacology***28**, 1017-1025 (2003).
60. U. Gärtner, C. Janke, M. Holzer, E. Vanmechelen, T. Arendt, Postmortem changes in the phosphorylation state of tau-protein in the rat brain. *Neurobiology of aging***19**, 535-543 (1998).

61. H. Tatebe *et al.*, Quantification of plasma phosphorylated tau to use as a biomarker for brain Alzheimer pathology: pilot case-control studies including patients with Alzheimer's disease and down syndrome. *Molecular Neurodegeneration***12**, 63 (2017).
62. S. Palmqvist *et al.*, Cerebrospinal fluid and plasma biomarker trajectories with increasing amyloid deposition in Alzheimer's disease. *EMBO Mol Med***11**, e11170-e11170 (2019).

Figures

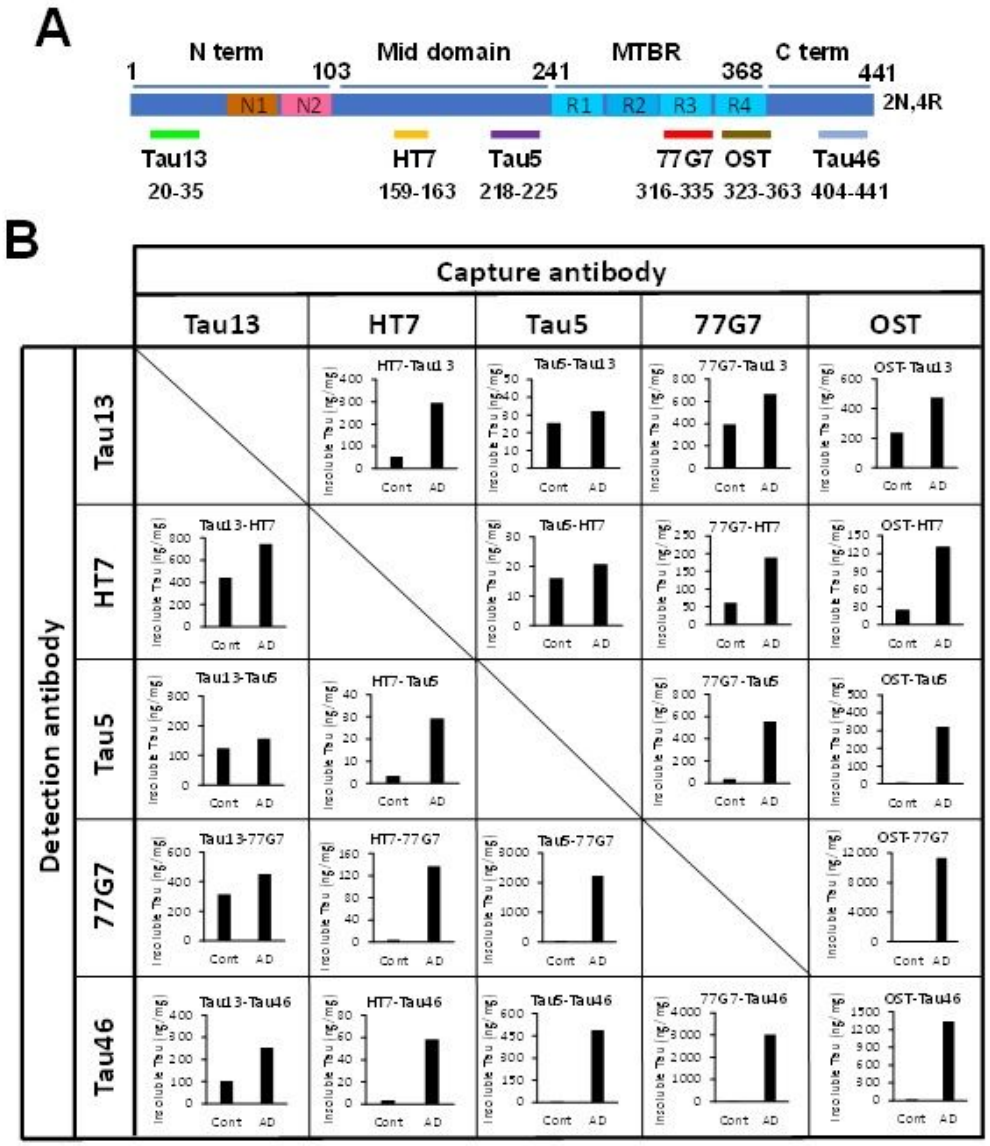

Figure 1

Distinct reactivity of tau ELISAs in evaluating pooled insoluble fractions of the frontal cortex from AD patients and non-AD control subjects. (A) Schematic representations of the longest tau isoform (2N4R) protein showing binding sites of tau antibodies used for the ELISAs in this study. (B) Reactivity of the pooled RIPA-insoluble fraction of the frontal cortex from control cases, and AD patients detected by each ELISA with a combination of the indicated capture and detection antibodies. MTBR = microtubule-binding region.

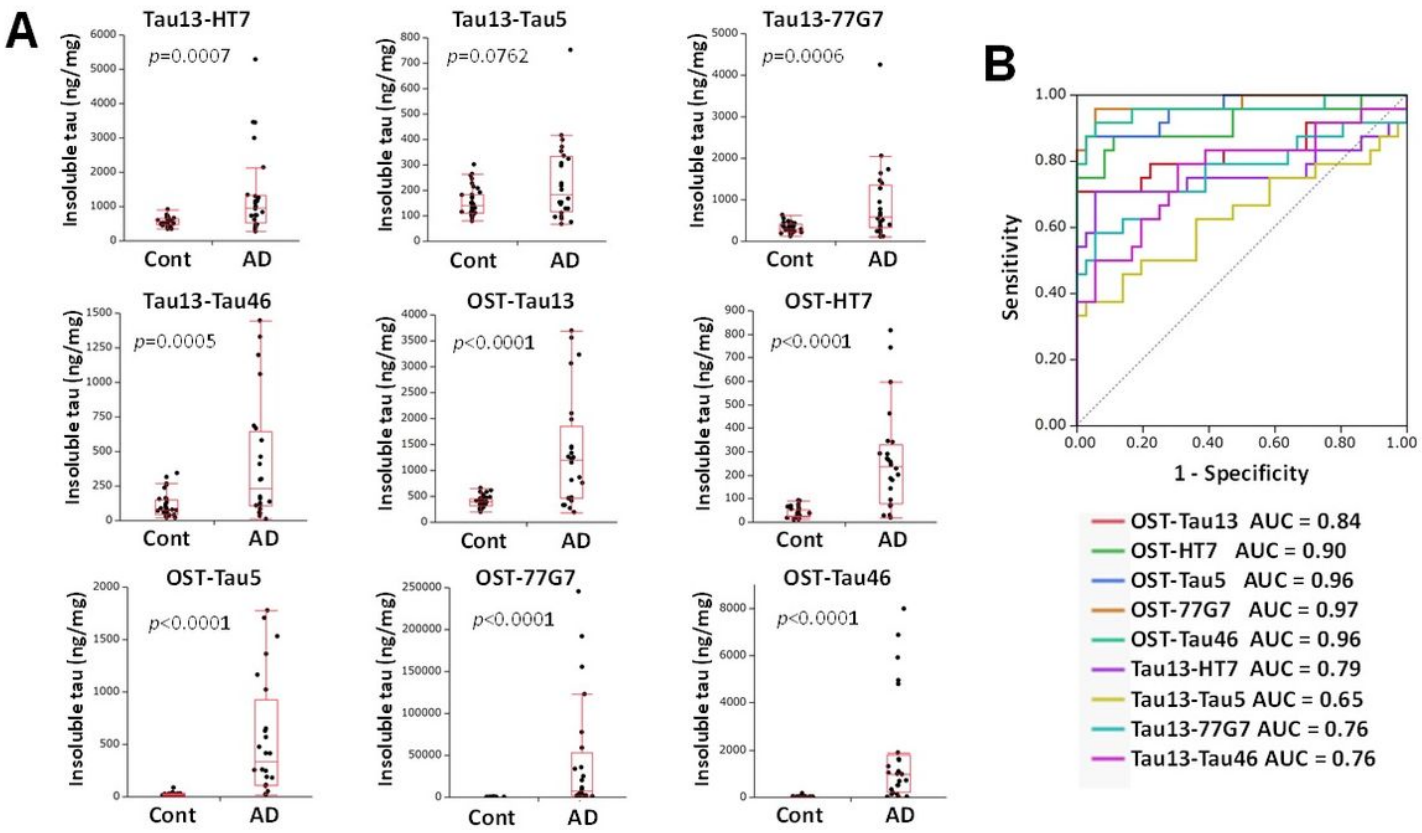

Figure 2

Distinct reactivity of tau ELISAs in evaluating the insoluble fractions of the frontal cortex of individual human brains. (A) Tau levels in the RIPA-insoluble fractions from non-AD controls, and AD patients detected by each ELISAs are plotted with a box-and-whisker diagram. P-values were acquired by the Wilcoxon rank-sum test. (B) ROC curve analysis of each tau ELISA for distinguishing AD patients and non-AD patients with AUC values.

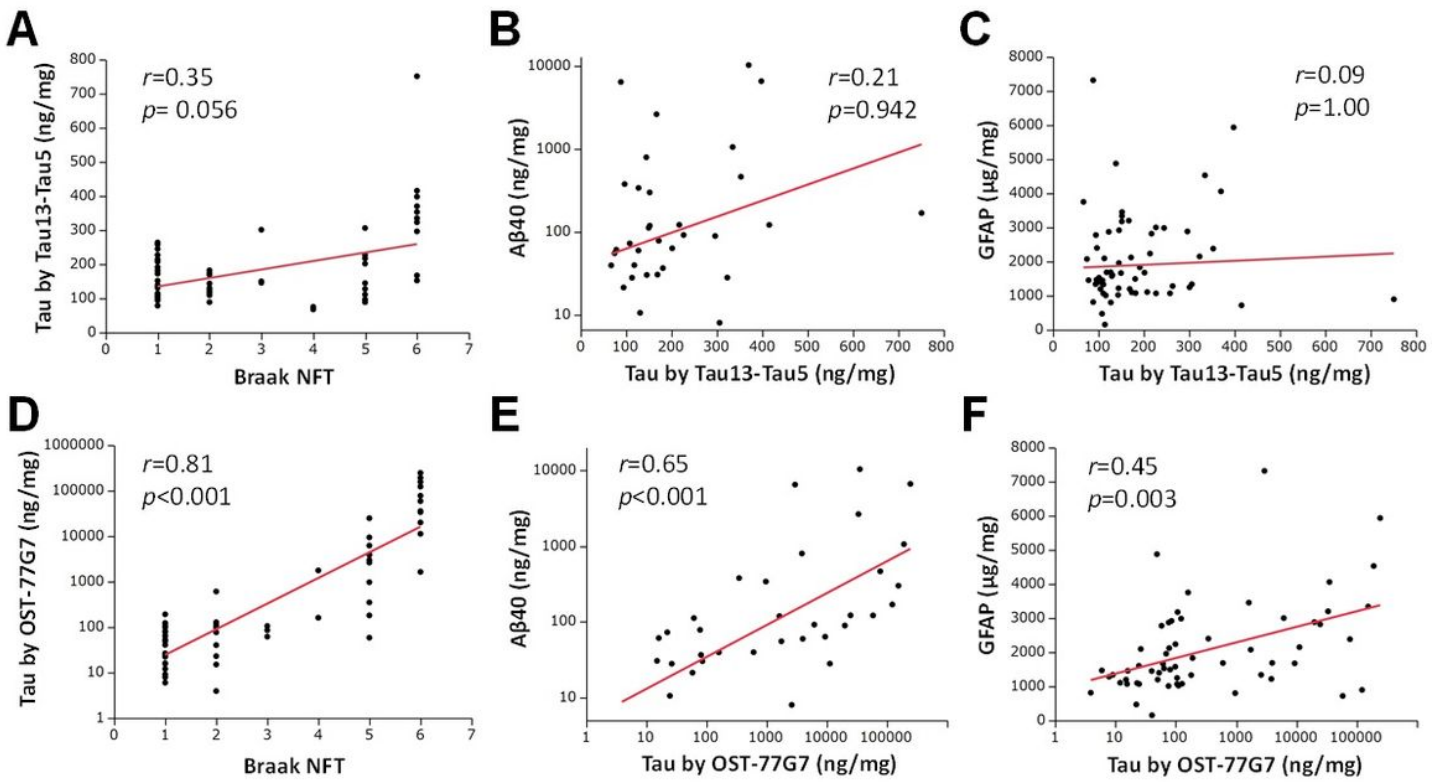

Figure 3

Correlation between AD pathologies and tau levels measured by each ELISA. (A-C) Tau levels in the RIPA-insoluble (GuHCl) fraction measured by Tau13-Tau5 ELISA are plotted against Braak NFT stage (A), Aβ40 levels in the GuHCl fraction (B), and GFAP levels (C). (B-D) Tau levels in the RIPA-insoluble (GuHCl) fraction measured by OST-77G7 ELISA are plotted against Braak NFT stage (D), Aβ40 levels in the GuHCl fraction (E), and GFAP levels (F). Correlation coefficient (r) and P-value were acquired by Spearman rank correlation test.

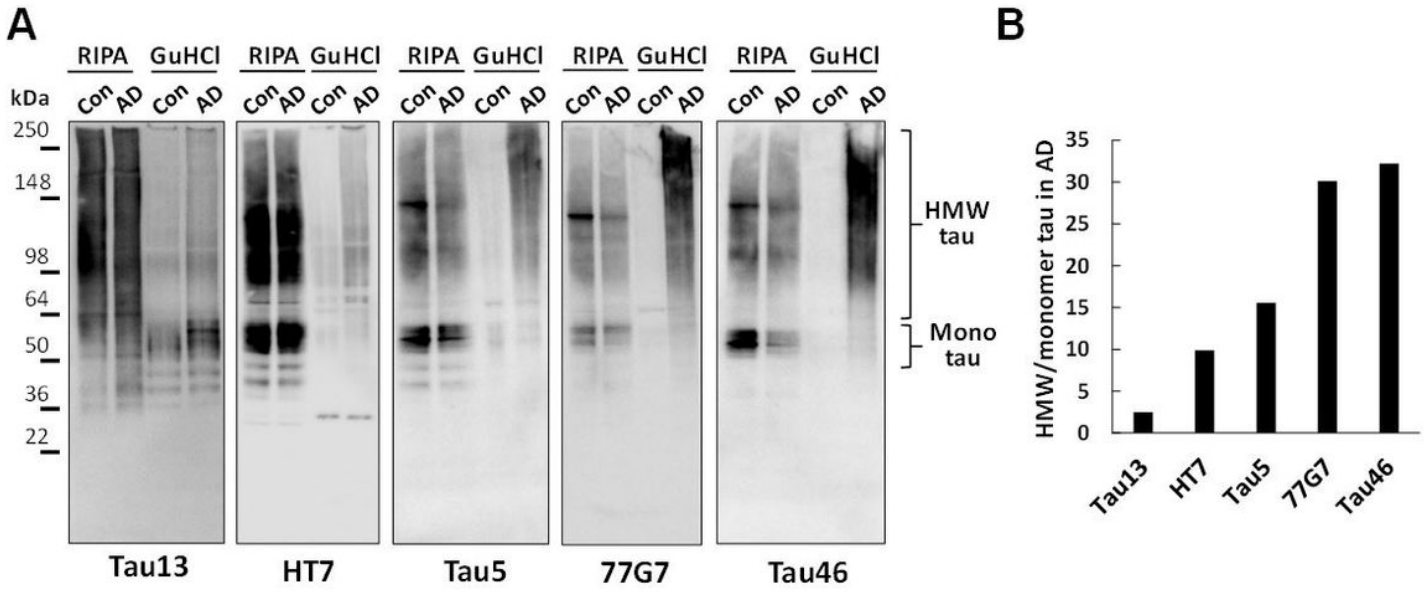

Figure 4

(A) Western blotting analysis of the pooled RIPA-soluble (RIPA) and RIPA-insoluble (GuHCl) fractions of human brains by the indicated tau antibodies. Aggregated tau (high molecular weight (HMW) tau) and monomer tau (Mono tau) are noted on the right side of the western blotting results. (B) Densitometric analysis of the ratio of HMW tau to monomer tau in the GuHCl fraction of the brains of AD patients.

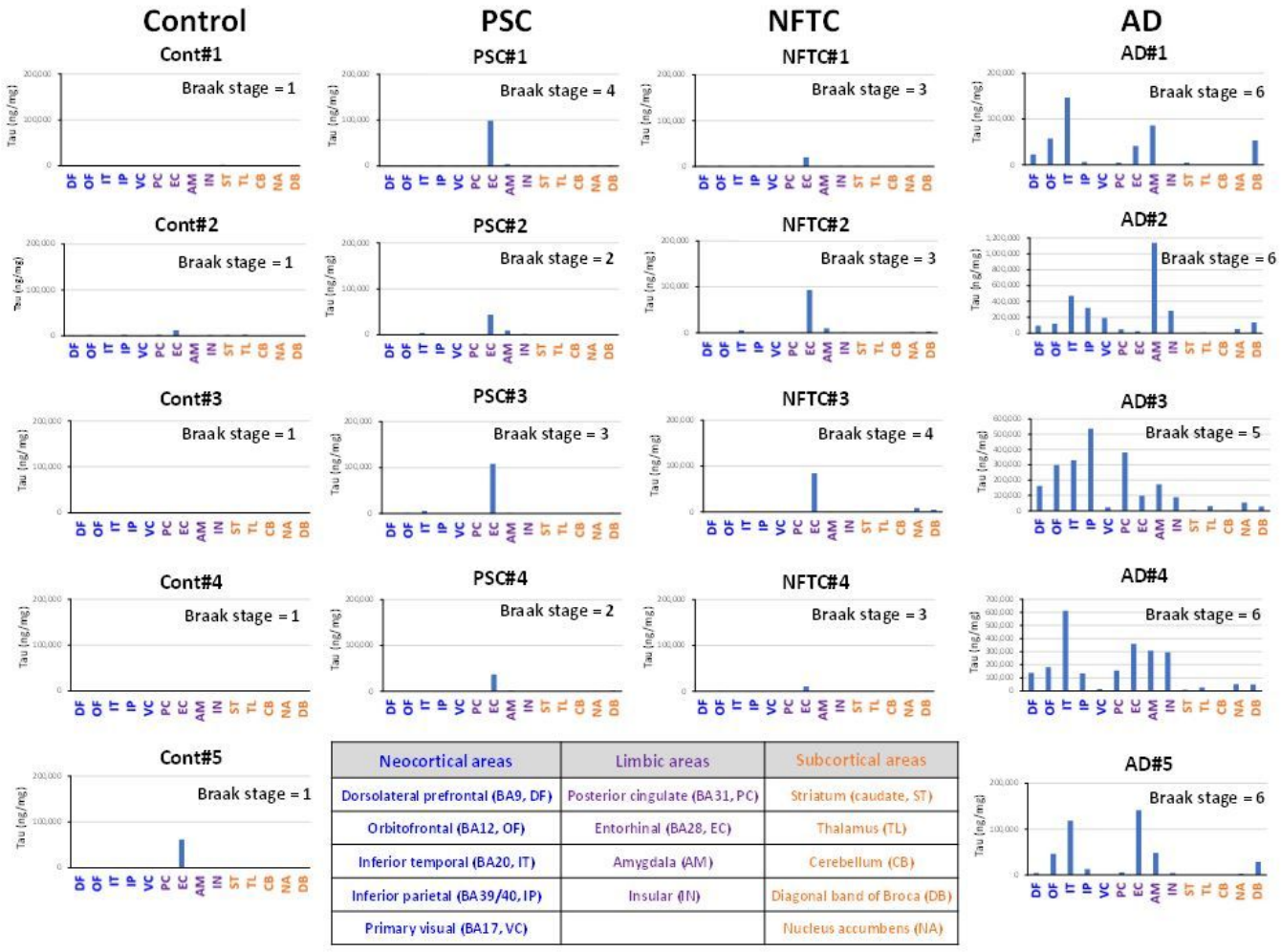

Neocortical areas	Limbic areas	Subcortical areas
Dorsolateral prefrontal (BA9, DF)	Posterior cingulate (BA31, PC)	Striatum (caudate, ST)
Orbitofrontal (BA12, OF)	Entorhinal (BA28, EC)	Thalamus (TL)
Inferior temporal (BA20, IT)	Amygdala (AM)	Cerebellum (CB)
Inferior parietal (BA39/40, IP)	Insular (IN)	Diagonal band of Broca (DB)
Primary visual (BA17, VC)		Nucleus accumbens (NA)

Figure 5

Amount of tau in the GuHCl fraction in 14 brain regions of individuals with PSC, NFTC, and AD, diagnosed by neuropathological assessment (Control = 5 subjects, PSC = 4 subjects, NFTC = 4 subjects, AD = 5 subjects), as measured by OST-77G7 ELISA. PSC = plaque dominant senile change, NFTC = NFT-predominant change. The inset table describes each brain region analyzed in the current study, stratified by neocortical areas, limbic areas, and subcortical areas. Blue notation indicates neocortical areas; purple notation indicates limbic areas; and orange notation indicates subcortical areas. The demographic information of each subject is described in supplementary Table 4.

Supplementary Files

This is a list of supplementary files associated with this preprint. Click to download.

- ShinoharaetalTauELISASupplementaryinformation.docx